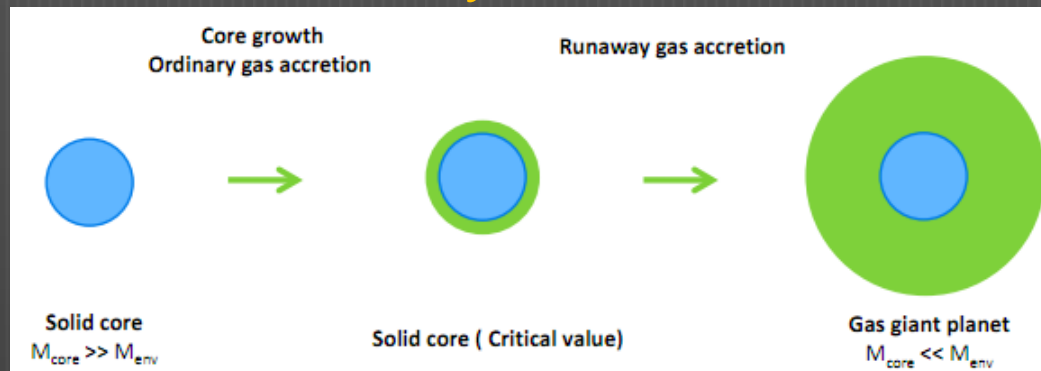


# The Relation of structure between the red giants and the gas giant planets

Kazuhiro KANAGAWA, Masayuki Y. FUJIMOTO ( Hokkaido University)

## ✓ Gas giant planet formation by core accretion model



## ✓ Structure analysis by UV homologues invariants

$$U \equiv \frac{d \log M_r}{d \log r} = \frac{4\pi r^3 \rho}{M_r}, \quad V \equiv -\frac{d \log P}{d \log r} = \frac{GM_r \rho}{rP},$$

- ◆ The structure change and the runaway accretion are related to the red giant structure of stars.
- ◆ The CCM is determined by three kinds of mechanisms.
- ◆ The magnitude of CCM depends strongly on the entropy at the bottom of envelope, the smaller the entropy, the smaller the critical core mass.

In the 1990s, CGRO/EGRET opened a new window in the high energy (MeV to GeV). These optical counterparts of gamma-ray sources are Pulsars, Blazars, globular cluster and so on. Specially, they found some normal galaxies and normal galaxies emitted gamma ray. In order to understand gamma ray radiation process, optical identify become important. Fermi satellite launched in 2008 and improved sensitivity, wide field of view ( $>2$  sr) and source location determination ( $<0.5'$ ). Fermi team published 1451 gamma ray sources detected by LAT/Fermi in the First Fermi-LAT catalog (1FGL) and half of them (630 source) are un-identified. We pick up 16 targets from 1FGL based on energy larger than  $1.5 \times 10^{11}$  erg/cm<sup>2</sup>/s and higher galactic latitude for expecting these targets will be high fraction to be AGN/Blazars. In the first step, we use color method to pick up blue color to be some candidates in the LAT 95% error region by using LOT/Lulin and Sloan Digital Sky Survey-Data Release 8 (SDSS-DR8). Second step, we use variability method to find short variability in these candidates by using LOT/Lulin and the Pan-STARRs that is a project for wide-field image. The most brightness one (1FGL J1231.1-1140) in our list is possible a Millisecond pulsar (MSP) (Maeda et. al 2011), and the PSR J1231-1411 has X-ray emission detected by SUZAKU. In our data, we don't detected optical emission in this error region is about  $7.44''$ . In the future, we will check variability for J1231-1411 in the Fermi error region to confirm it's MSP and we will finish data analysis for these 16 targets to find possible type of gamma ray source.

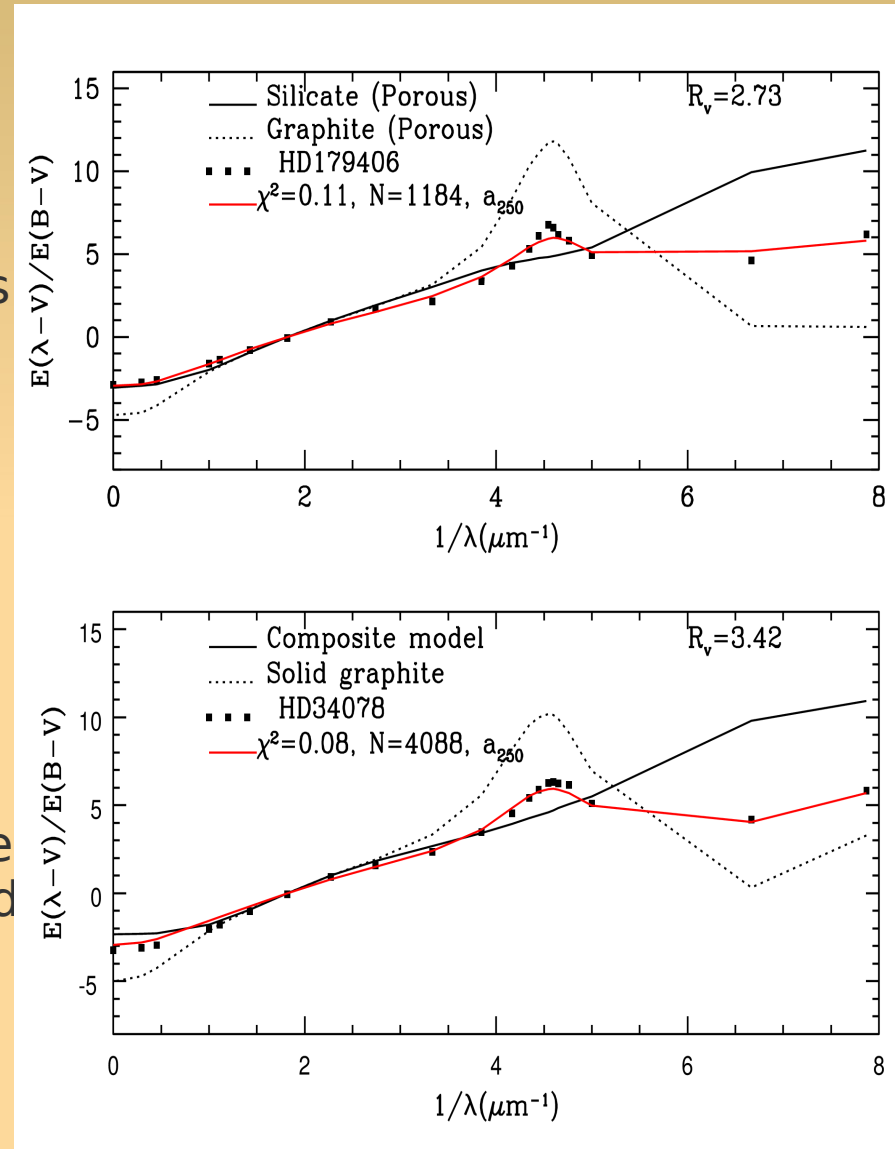
# Interstellar Dust Models towards some IUE stars

Nisha Katyal<sup>1</sup>, Ranjan Gupta<sup>1</sup>, D B Vaidya<sup>2</sup>

<sup>1</sup>Inter University centre for Astronomy and Astrophysics (IUCAA), Pune, India

<sup>2</sup>ICCSIR, Ahmedabad, India

- We study the extinction properties of 26 IUE stars lying in various dust environments. Variation in shape of extinction curves provides insight about grains along the sight lines.
- These stars are modeled with the help of porous and composite spheroidal grain models generated using DDA.
- Composite spheroidal grain models, with axial ratios 1.33 & 2.00 and volume fraction of inclusions 0.1-0.3, fit 14 observed extinction curves reasonably well (eg. HD34078).
- The porous spheroidal grain models with different porosities viz.  $P=0, 0.5$  &  $0.7$  and same axial ratio ( $AR=1.33$ ) fit the remaining observed extinction curves quite satisfactorily (eg. HD179406).
- From the sample of 26 observed IUE stars, about 88% fit the model curves with larger size distribution,  $a=0.005-0.250\mu$  ( $a_{250}$ ).



Fitting of observed extinction using two different types of models viz porous and composite model.

# Observations of Far-Ultraviolet Diffuse Emission from the Small Magellanic Cloud

Ananta C. Pradhan, Jayant Murthy and Amit Pathak  
Indian Institute of Astrophysics, Bangalore - 560 034, India

● **Far-ultraviolet diffuse radiation** is primarily due to radiation from hot stars scattered from the interstellar dust grains.

● **Small magellanic Cloud (SMC)** is a nearby extragalactic object where dust is known to be different.

● **Data Analysis:** Used CalFUSE v3.2 and data analysis of [Murthy & Sahnow \(2004\)](#) and obtained 30 diffuse observations out of 220 Far-ultraviolet Spectroscopic Explorer (FUSE). We have also used Ultraviolet Imaging Telescope (UIT) data in order to estimate the FUV diffuse fraction.

## Result & Discussion

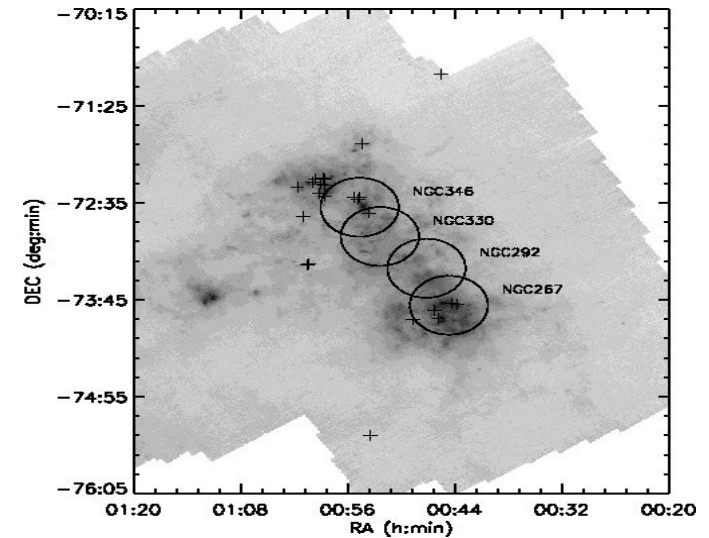
● We report the first observations of far-ultraviolet (FUV: 1000 – 1150 Å) diffuse radiation from the SMC.

● The strength of FUV diffuse surface brightness in the SMC ranges from 2000 to  $3 \times 10^5$  photons  $\text{cm}^{-2} \text{s}^{-1} \text{sr}^{-1} \text{Å}^{-1}$  at 1004 Å.

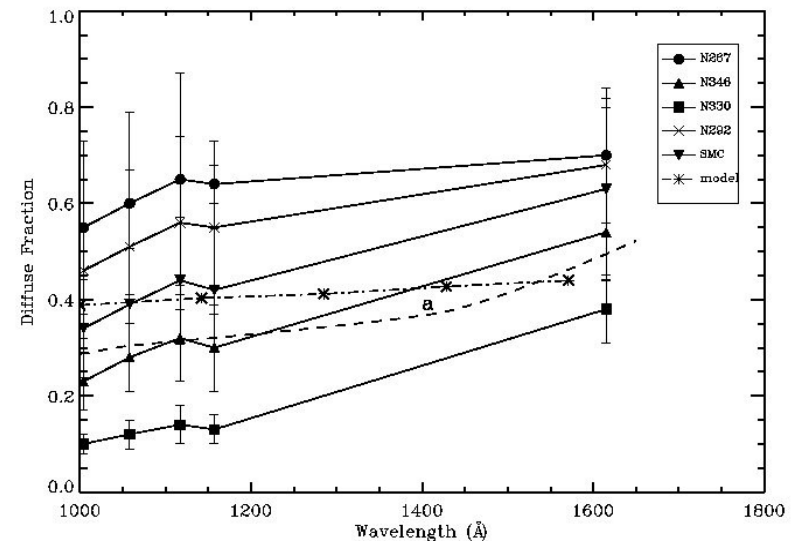
● The contribution of diffuse emission to the total radiation field was found to be 34% - 44% at FUSE bands increasing up to 63% at 1615 Å.

● The amount of light scattered increases towards the longer wavelengths showing that a large percent of the light at shorter wavelengths is absorbed by the dust.

● There is a difference between the FUV diffuse fraction from the SMC and the Large Magellanic Cloud (LMC) with the SMC fraction being higher probable because the higher dust albedo.



SMC Map with FUV Diffuse Observations



Variation of FUV diffuse fraction with Wavelengths

# Isophotal shapes of early-type galaxies to very faint levels

Laxmikant Chaware<sup>1</sup>, Ajit K. Kembhavi<sup>2</sup>, Russell Cannon<sup>3</sup>, Ashish Mahabal<sup>4</sup> and S. K. Pandey<sup>1</sup>

<sup>1</sup>Pt. Ravishankar Shukla University, Raipur; <sup>2</sup>Inter-University Centre for Astronomy and Astrophysics, Pune;

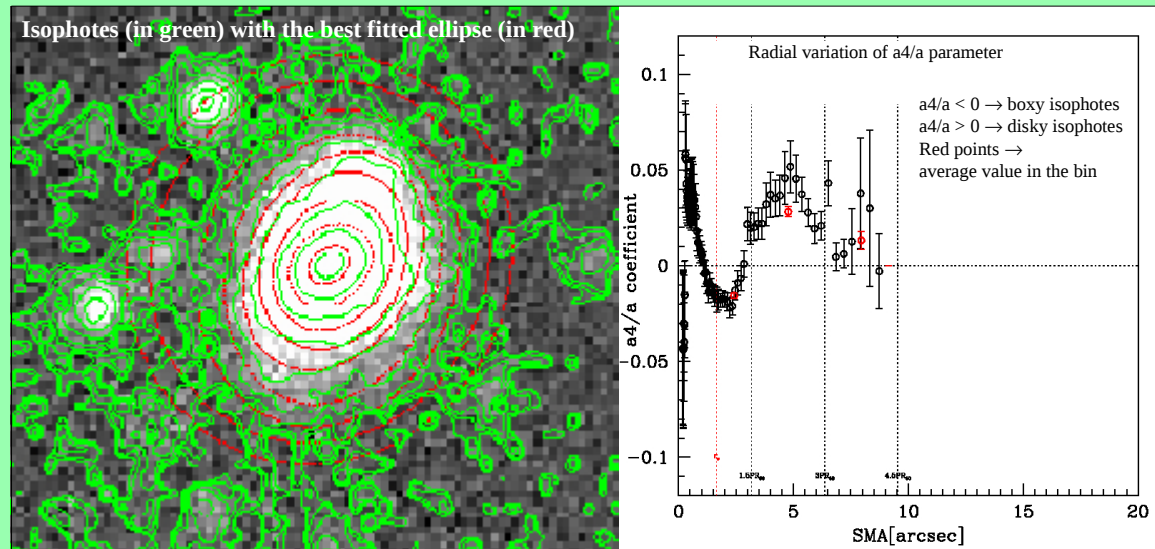
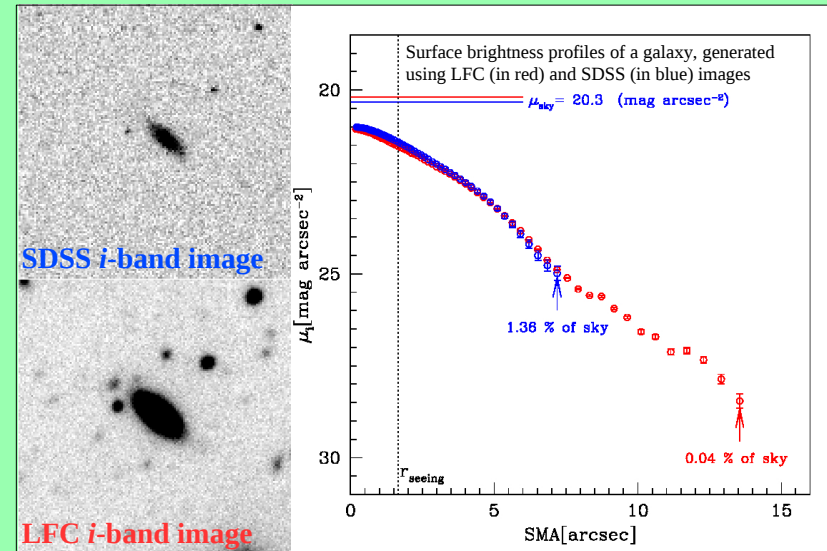
<sup>3</sup>Anglo-Australian Observatory, Australia; <sup>4</sup>California Institute of Technology, Pasadena

The study of isophotal shapes of early-type (E/SO) galaxies is important as the galaxies having boxy (rectangular) isophotes are known to have different physical properties as compared to the galaxies having disk (pointed) isophotes.

Deep images of 132 sample galaxies obtained from Large Format Camera (LFC) on Palomar 5m Hale telescope is used to explore the region of galaxies which is largely inaccessible through short exposure.

We derive average values of isophotal shape parameters in four different radial bins along the semi-major axis of a galaxy, instead of assigning a single global characteristic value of a parameter for the galaxy as done by earlier researchers studying isophotal shapes.

We find that the isophotal shapes of inner regions of our sample galaxies are statistically different from the isophotal shapes observed at outer regions. This has important implications for theories of galaxy formation and evolution as it suggests that outer and inner part of the early-type galaxies might not have co-evolved



# VARIABILITY OF ULTRA-LUMINOUS X-RAY SOURCES

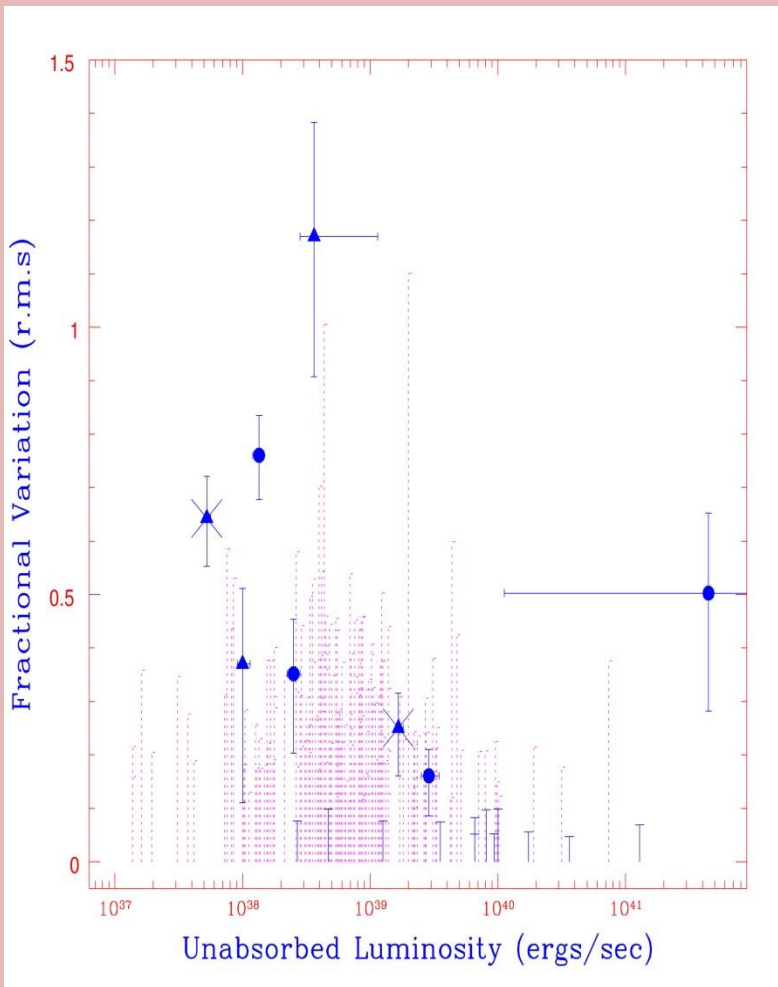
SOMA MANDAL <sup>1</sup>, RANJEEV MISRA <sup>2</sup>

<sup>1</sup> TAKI GOVERNMENT COLLEGE, WEST BENGAL, INDIA

<sup>2</sup> INTER-UNIVERSITY CENTRE FOR ASTRONOMY AND ASTROPHYSICS ( IUCAA), INDIA

Ultra-Luminous X-ray Sources (ULXs) are point like non-nuclear X-ray sources with Luminosity  $L_x > 10^{39}$  erg/sec

- Chandra observations of 17 nearby galaxies were analyzed
- 166 sources were chosen for temporal analysis
- Extracted light curves for time bin of 4 ksec
- Variance is computed to differentiate the variable and non-variable one



❖ 8 sources were found to be variable

❖ Three are ULXs

❖ ULX are typically not highly variable in ksec time scales, except for some ultra-soft one

# Soft X-Ray Time lag Behaviour of Mrk 1040

Shruti Tripathi<sup>1</sup>, Ranjeev Misra<sup>2</sup>, Gulab Dewangan<sup>2</sup>, Shantanu Rastogi<sup>1</sup>

<sup>1</sup>DDU Gorakhpur University, Gorakhpur-273 009

<sup>2</sup>Inter-University Centre for Astronomy and Astrophysics, Pune-411 007

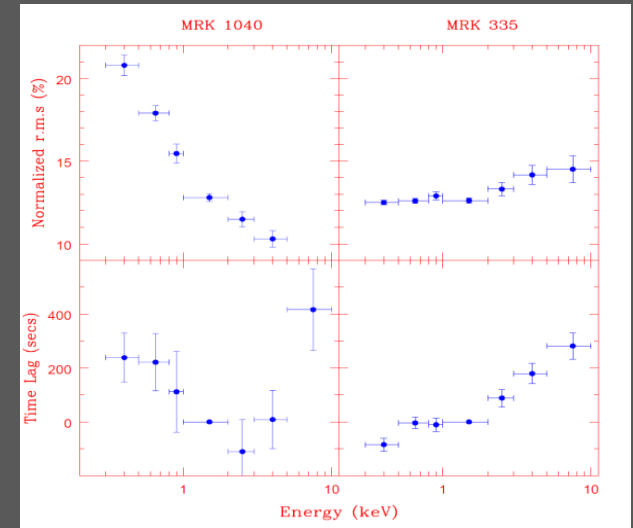
❖ Temporal studies of Active Galactic Nuclei show that hard flux changes after the soft flux. The reverse behaviour or soft lag is observed only in few cases.

❖ We analysed a XMM-Newton observation of Mrk 1040 which seems to show soft lags on the dominant variability timescale of  $10^4$  s.

❖ Two different scenarios may account for soft time lag.

One is the reverberation effect of a relativistically blurred reflection component responding to a varying continuum. Another possibility could be due to Comptonization delays when high energy photons impinge back on the soft photon source.

❖ Application of either model will help in constraining the radiative processes, geometry and more importantly the size of the system and provide an opportunity to test strong General Relativistic effects.



The r.m.s variability and the time lag as a function of energy for Mrk 1040 and Mrk 335.

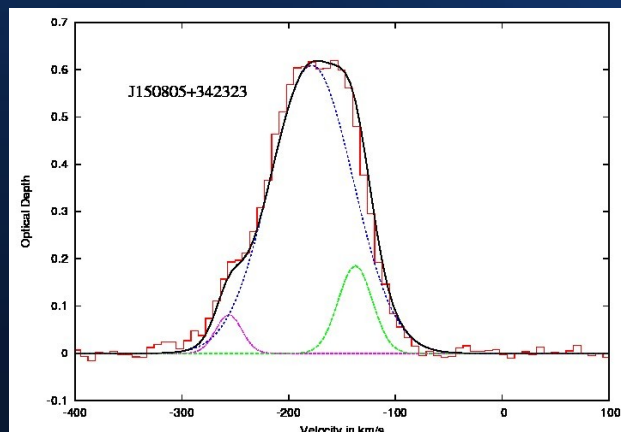
# HI absorption towards nearby compact radio sources

Yogesh Chandola, S. K. Sirothia and D. J. Saikia, 2011, MNRAS (in press), arXiv:1108.2242



**AIM** To study **HI absorption features** in a sample of **low luminosity** ( $< 10^{25}$  W/Hz at 5GHz), nearby Compact Steep Spectrum (**CSS**) and Giga-Hertz Peaked Spectrum (**GPS**) radio sources.

**SAMPLE and OBSERVATIONS** We observed the **CORALZ** (Compact Radio Sources at Low Redshift) sample of **18 sources** using the **GMRT**. These sources are of **lower luminosity than earlier studies** of CSS and GPS objects. The spectral resolution is  $7 \text{ km s}^{-1}$  and channel rms is  $1.3 \text{ mJy}$ .



Optical depth vs. velocity in  $\text{km s}^{-1}$  relative to optical systemic velocity for J150805+3423 (one of the 7 sources for which HI absorption has been detected).

**RESULTS and CONCLUSIONS** We found **7 new cases of HI absorption**, out of which 3 are GPS and 4 are CSS sources. The **detection rate in GPS (~50%)** is higher than **CSS (~36%) sources**, similar to **higher luminosity objects**.

There appears to be no evidence of any dependence of HI column density on either luminosity or redshift, but **is consistent with the known inverse relation of HI column density with projected linear size**.

The **relative velocity of the blueshifted absorption features**, which may be due to jet-cloud interaction, **extend to only ~250  $\text{km s}^{-1}$**  for these CORALZ sample compared with values of over  $\sim 1000 \text{ km s}^{-1}$  for the more luminous CSS and GPS objects. This could be due to weaker jets in these low luminosity sources, although this needs confirmation from a larger sample of objects.

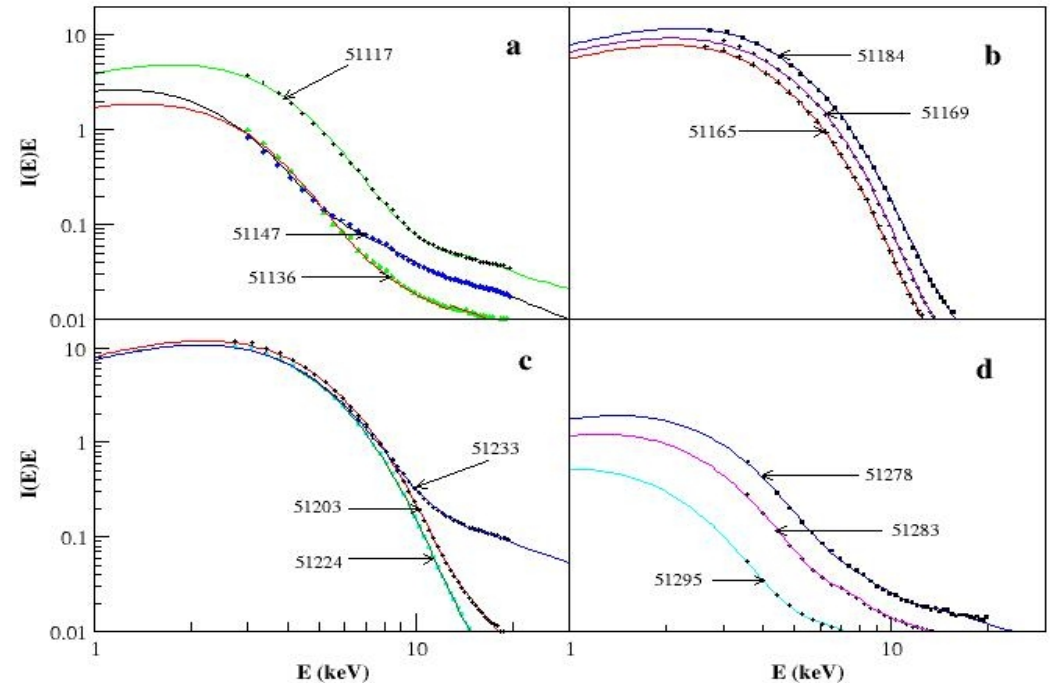
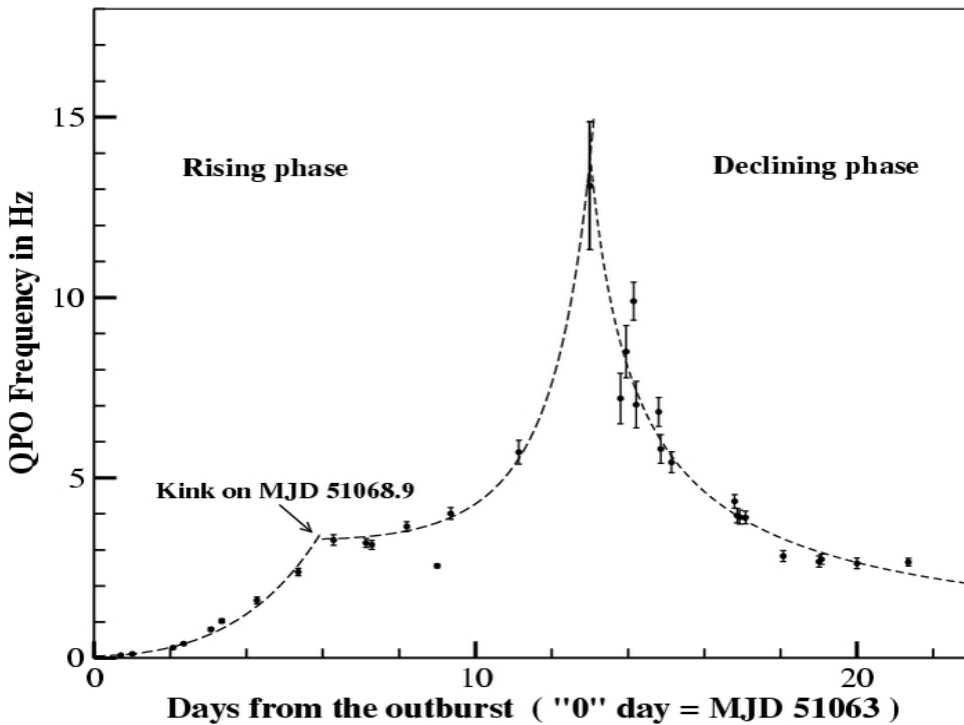


# Evidence of Two component flows around the Galactic black hole candidates during their outbursts

Broja Gopal Dutta<sup>1,2</sup>

1. Y. S. Palpara College, Purba-Medinipur, West Bengal, 721458, India

2. Indian Centre for Space Physics, Kolkata, 700084, India



1. We observed systematic drift in QPO frequency ( Sept.7 to Sept.19). It increased from 81mHz to 13.1 Hz and immediately started to decrease & became 2.62 Hz on Sept. 26) and matches satisfactorily with propagatory oscillating shock solution.

2. The Keplerian rate, sub-Keplerian rate and CENBOL size are governing the entire spectral states of the GBHCs.

# Entropy Changes in the Clustering of Galaxies in an Expanding Universe

<sup>1</sup>Tabasum Masood, <sup>1, 2</sup> Naseer Iqbal, <sup>1</sup> M.S.Khan

<sup>1</sup> Department of Physics, University Of Kashmir, Srinagar, India.

<sup>2</sup> Interuniversity Centre for Astronomy and Astrophysics, Pune, India

## Thermodynamic Description of Galaxy Clusters:

$$U = \frac{3NT}{2} (1 - 2b)$$

$$P = \frac{NT}{V} (1 - b)$$

$$b = -\frac{W}{2K} = 2\tau Gm^2 \frac{n}{3T} \int_0^\infty \xi(\bar{n}, T, r) r dr$$

## . Entropy Calculations:

The grand canonical partition function is given by:

$$Z_N(T, V) = \frac{1}{N!} \left( \frac{2\pi mkT}{\Lambda^2} \right)^{\frac{3N}{2}} V^N [1 + \beta \bar{n} T^{-3}]$$

$$S - S_0 = - \left[ \frac{1}{2} \ln \bar{n} + \frac{1}{2} \ln [b(1-b)] + 3b \right]$$

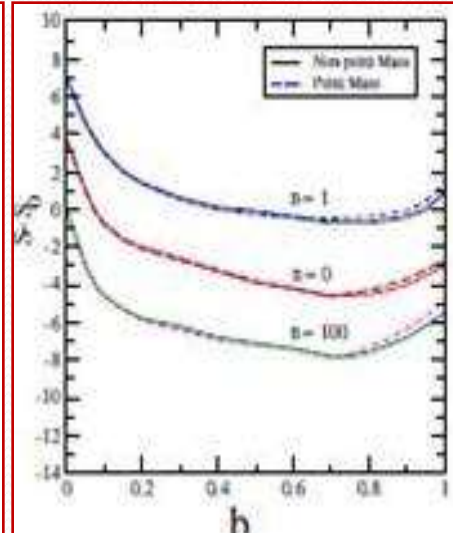
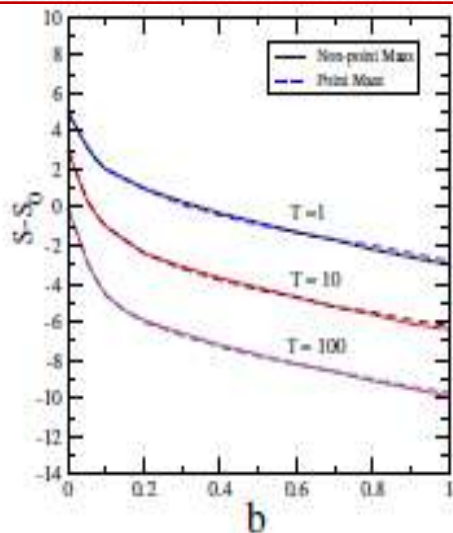
$$S - S_0 = - \left[ 3b + \ln (bT^{\frac{3}{2}}) \right]$$

$$S - S_0 = - \left[ \ln \frac{bT^{\frac{3}{2}}}{1 + b(\alpha - 1)} + \frac{3b\alpha}{1 + b(\alpha - 1)} \right]$$

$$S - S_0 = - \left[ \frac{1}{2} \ln \bar{n} + \ln \frac{[b(1-b)]^{1/2}}{1 + b(\alpha - 1)} + \frac{3b\alpha}{1 + b(\alpha - 1)} \right]$$

Results:

Study of entropy results given by above equations shows that the entropy of universe decreases first with the clustering rate of the particles and then gradually increases as the system attains virial equilibrium.





# Structure and Stability of X-Ray Irradiated Accretion Disk



<sup>1</sup>Bari Maqbool, <sup>2</sup>Ranjeev Misra, <sup>3</sup>Naseer Iqbal, and <sup>4</sup>Gulab Dewangan

1, 3 Department of Physics, University of Kashmir, Srinagar, India.

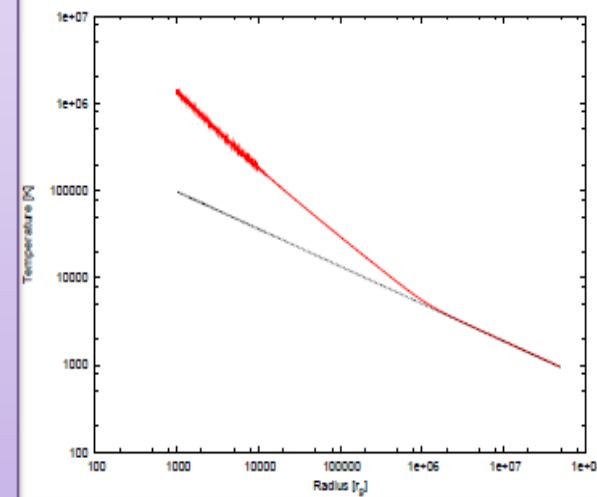
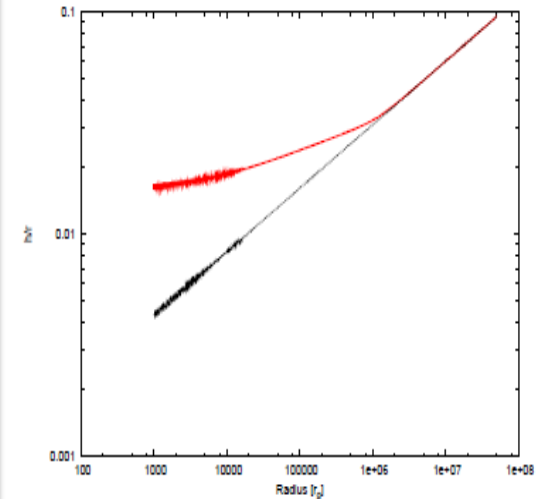
2,4 Inter-University Centre for Astronomy and Astrophysics, Pune, India

❖ When the mass accretes on to the compact star, the X-Rays emitted hit and change the behavior of the outer region of the Accretion Disk.

❖ We are concerned here with finding the structural changes that occur in the outer region due to X-ray irradiation and also study the stability of such a disk.

❖ There is a sharp transition, as we go from the X-ray Irradiated region to the region where X-Ray Irradiation is not important. This transition point, called as *Transition Radius*.

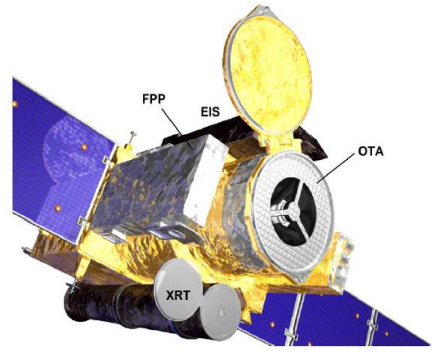
❖ Our calculations show that the X-Ray Irradiation will be significant only in those Low Mass X-Ray Binaries in which outer disk radius is larger than the transition radius.



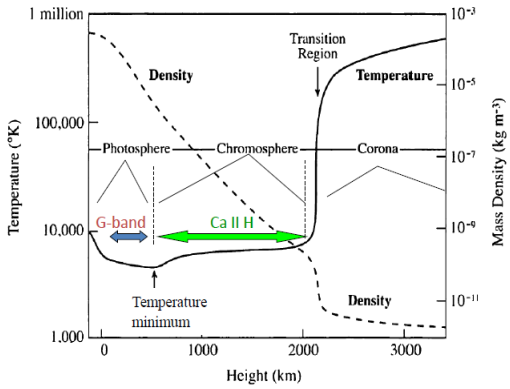
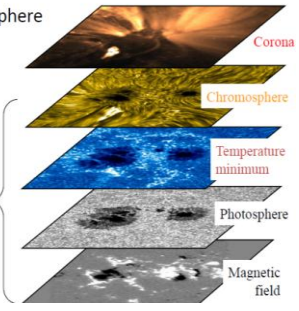
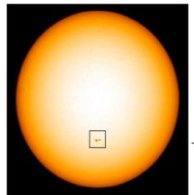


**Observations of Solar Chromosphere with Hinode**  
 K. Alkendra P. Singh  
 (singh@kwasan.kyoto-u.ac.jp)  
 Kwasan & Hida Observatories, Kyoto University  
 Yamashina, Kyoto 607-8471, Japan

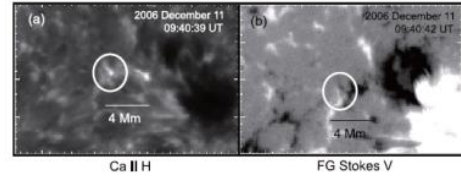
**Collaborators:**  
**Hiroaki Isobe, USSS**  
**N. Nishizuka, ISAS**  
**K. Shibata, Kyoto**



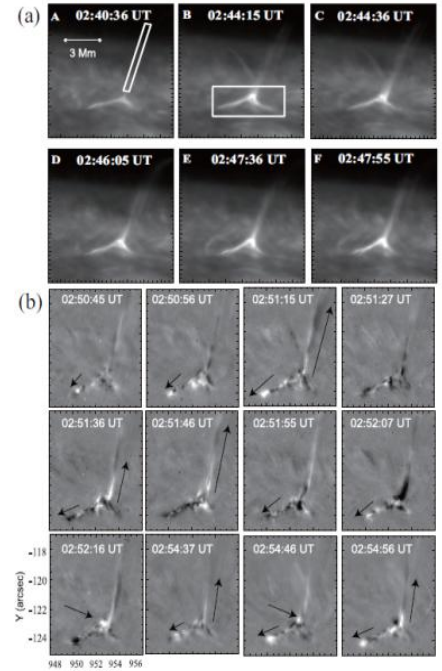
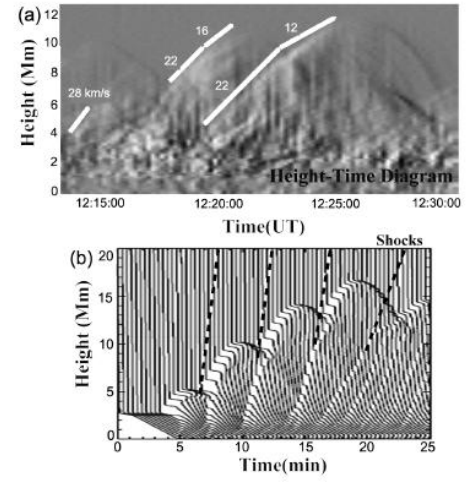
The Solar Optical Telescope (SOT) on Hinode observes photosphere & chromosphere



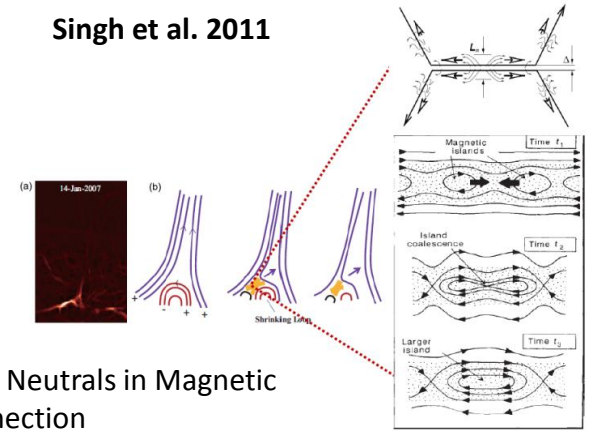
Shibata et al. 2007, Science



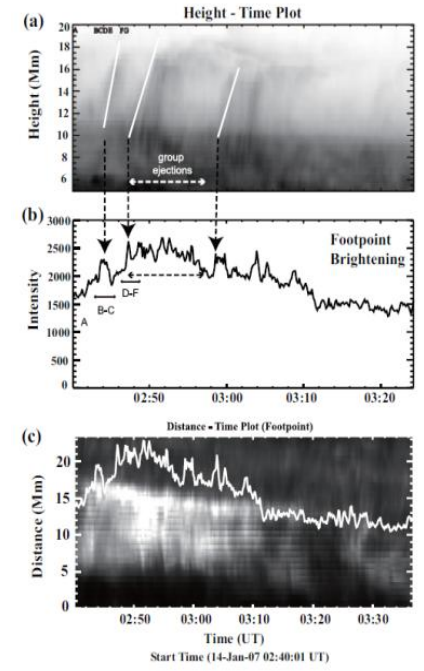
Nishizuka et al. 2010



Singh et al. 2011

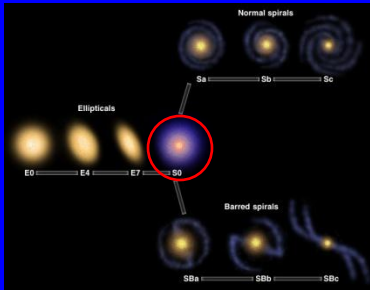


Role of Neutrals in Magnetic Reconnection



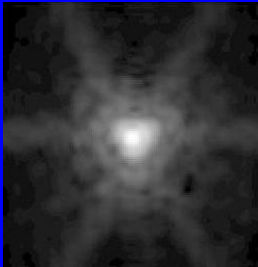
# Point Spread Function of Spitzer IRAC Mosaics for 2-D Decomposition of Galaxy Images

- Kaustubh Vaghmare (IUCAA, India)



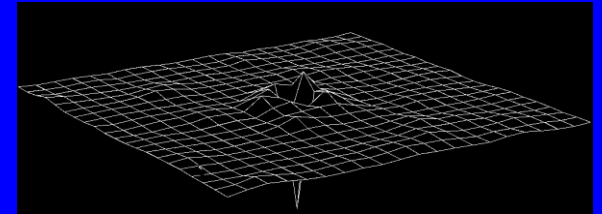
Are lenticular galaxies just an intermediate stage between ellipticals and spirals? Or are they a class in their own right?

As a part of a multi-wavelength study of lenticulars, we wish to perform 2-d surface photometry of lenticular galaxies using 3.6 micron IRAC images from the Spitzer Space Telescope.

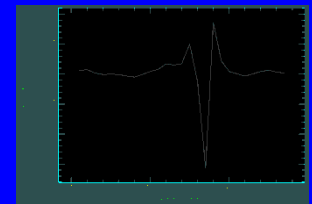


The determination of an accurate Point Spread Function is crucial for accurate 2-d surface photometry.

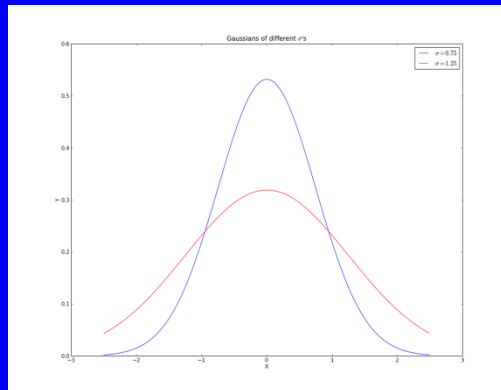
But since data from IRAC is severely under-sampled, we have to use the PSF library made by Spitzer Science Centre.



But these PSFs are not suitable for IRAC mosaics and are meant for IRAC CCD images as shown from residue analysis obtained by fitting stars with the PSFs.



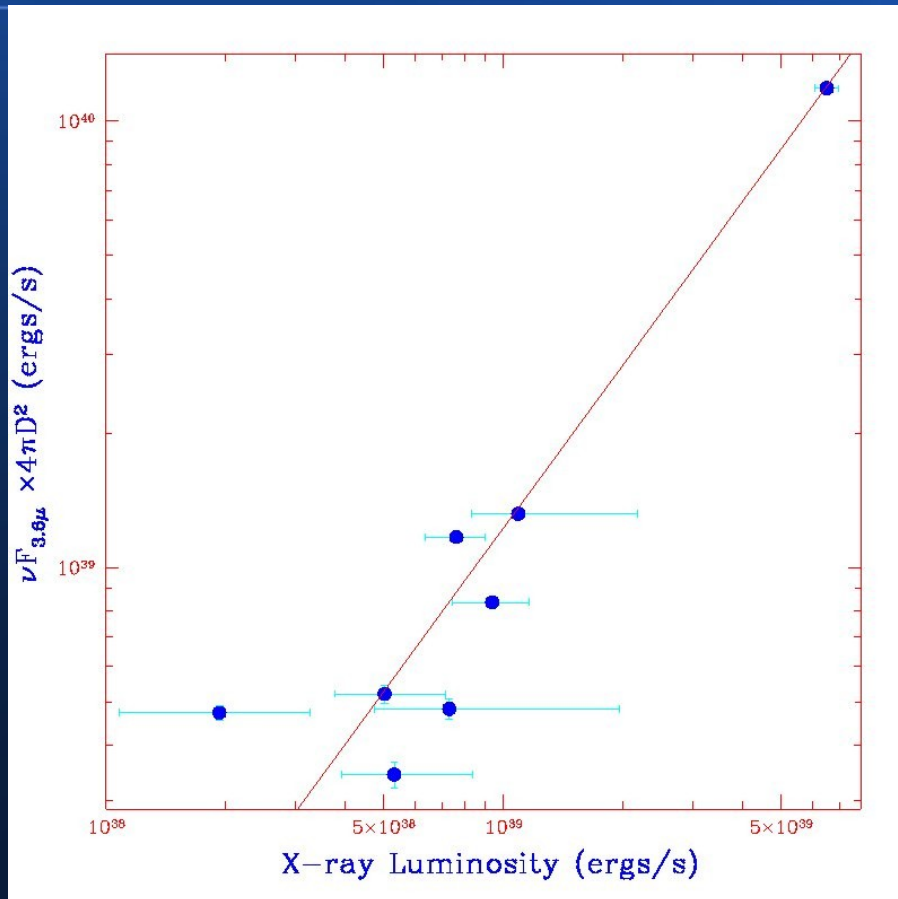
Residue data is consistent with FWHMs of CCD and Mosaic images being mismatched. The process of mosaic construction broadens out the PSF.



When the PSF is modified by convolving it with a Gaussian, whose properties are determined from field stars, the PSF gets appropriately broadened out. The residue levels improve from ~13% in the previous case down to ~4% which is at a level of background fluctuations. It is very important in 2-d decomposition that FWHM of data and PSF should match, especially for determining bulge parameters.

# Mid-Infrared counterparts of X-ray sources in NGC1399

-*Shalima P<sup>1</sup>, Jithesh V.<sup>2</sup>, Jeena K.<sup>3</sup>, R. Misra<sup>1</sup>, S. Ravindranath<sup>1</sup>, G. Dewangan<sup>1</sup>, C. D. Ravikumar<sup>2</sup>, B. R. S. Babu<sup>2</sup>*



- NGC1399 is an elliptical galaxy that hosts a large number of X-ray point sources
- MIR counterparts of X-ray point sources are detected using Spitzer IRAC
- IRAC 5.8/3.6 colours used to classify the sources
- 8 sources had AGN-like IRAC colours
- IR-X-ray correlation coefficient of 0.86 for AGN-like sources
- SEDs derived for all sources

1 - IUCAA

2 - Calicut University

3 - Providence Women's College, Calicut

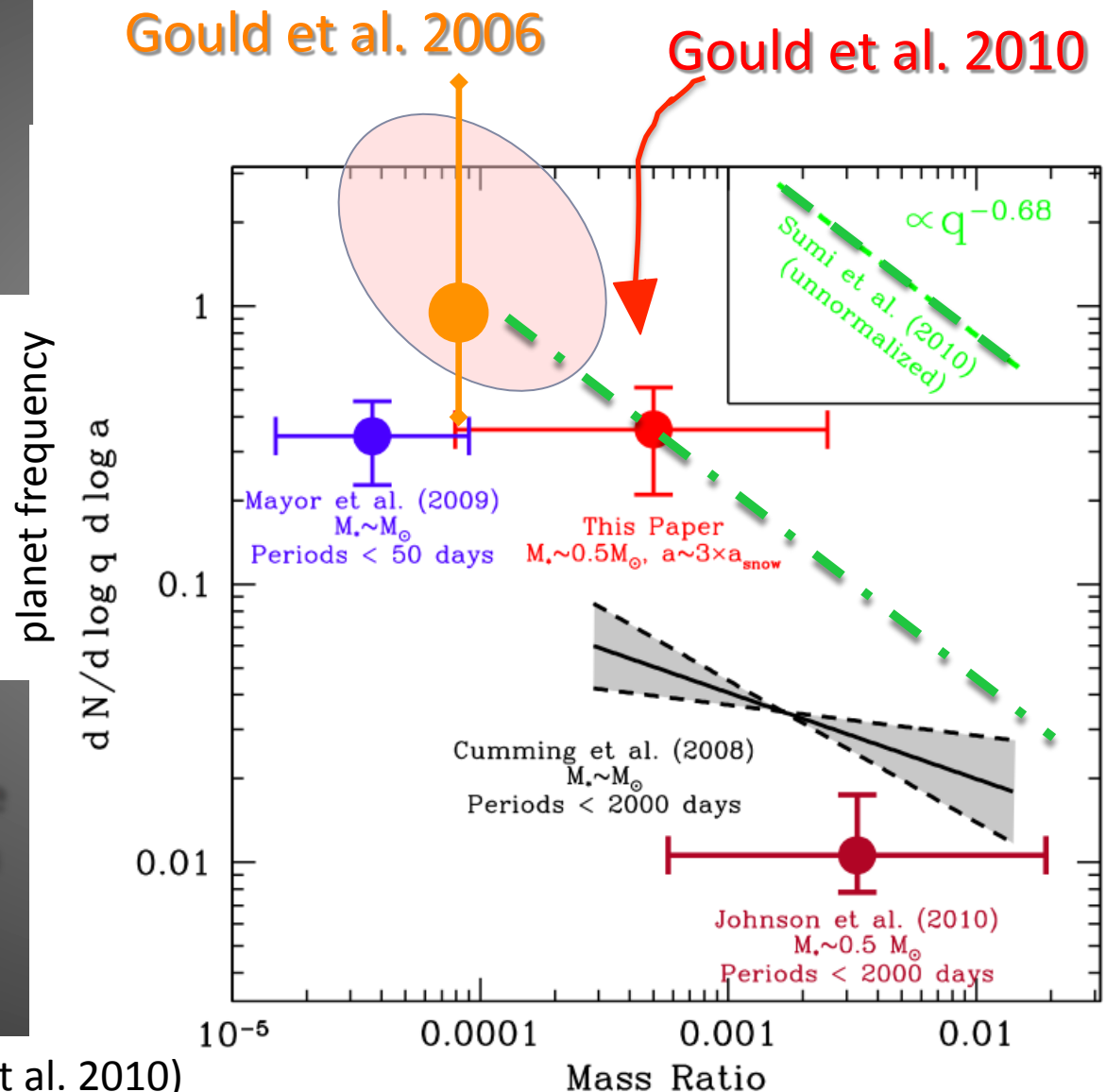
# Detection efficiency of planets in the low magnified gravitational microlensing events

Daisuke Suzuki (Osaka Univ.)

- The half of the planetary events are found in the low-mag event.
- The low-mag events are more sensitive to the planets of smaller mass ratio.

To estimate the planet frequency beyond the snow line we have to derive the detection efficiency precisely with low-mag events !

(Gould et al. 2010)



# RXTE Observations of LMXB XTE J1701-407; new possible outburst

D. Pawar<sup>1</sup>, M. Kalamkar<sup>2</sup>, D. Altamirano<sup>2</sup>, K. Shanthi<sup>3</sup>, D. Bhattacharya<sup>4</sup>

<sup>1</sup>R.J. College, Mumbai, India; <sup>2</sup>Universiteit van Amsterdam; <sup>3</sup>UGC-ASC, University of Mumbai; <sup>4</sup>IUCAA, Pune, India

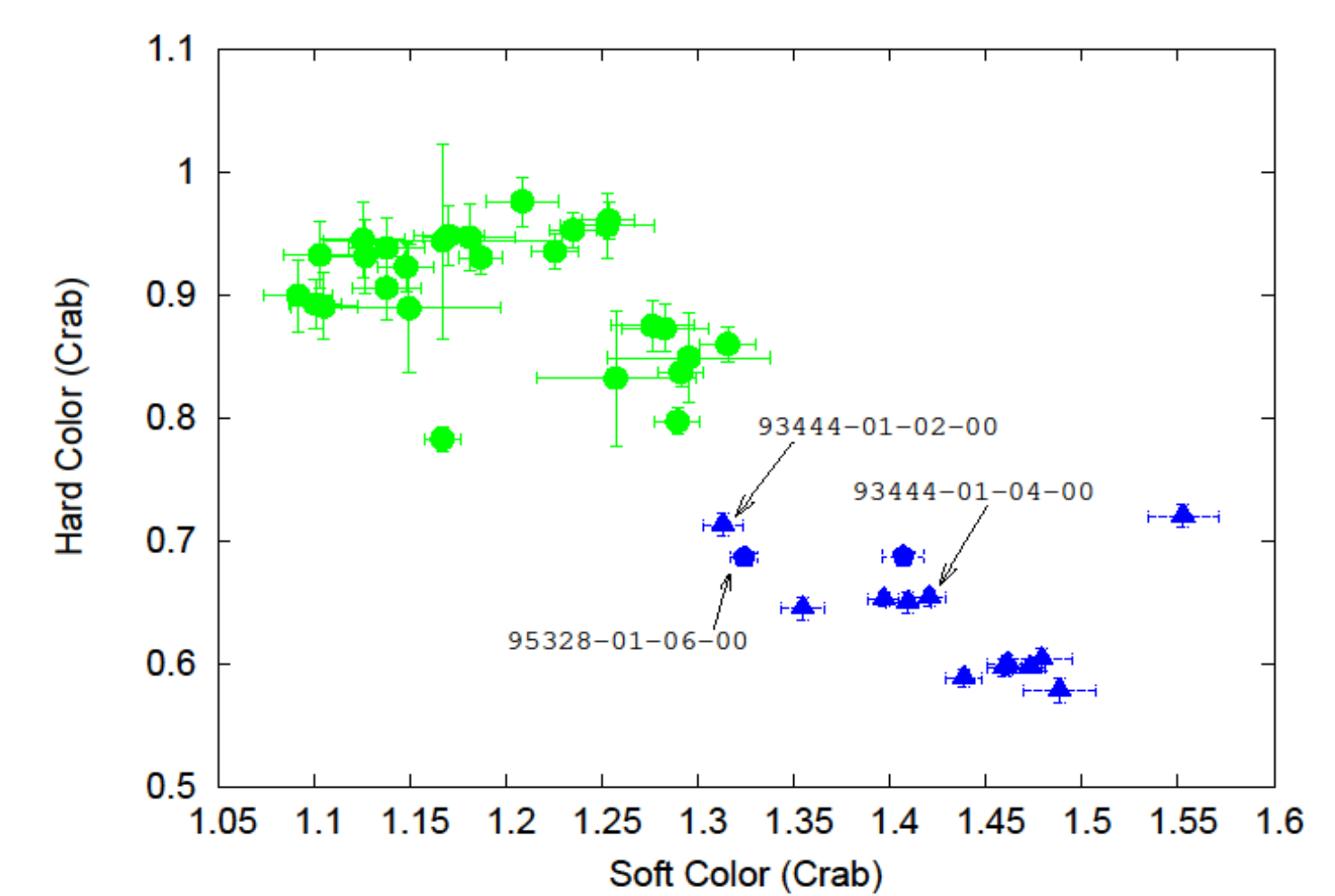
We report the detection of kHz quasi periodic oscillations (QPOs) in the Rossi X-ray Timing Explorer (RXTE) observations of the low mass x-ray binary (LMXB) XTE J1701-407. The source behaviour in the colour-colour diagram and its power spectra indicates the atoll nature of the source. The kilohertz QPOs were detected when the source was in a soft high-intensity state. A QPO of frequency  $1156 \pm 3.6$  Hz was detected in one observation. The fractional root mean square (rms) of this QPO ( $\sim 30\%$ ) is one of the highest observed amongst known atoll sources. Twin QPO peaks were detected twice in observations separated by  $\sim$ two years. Their frequencies  $\sim 742 \pm 3.4$  Hz and  $\sim 1133 \pm 8.9$  Hz. The frequency difference of  $372 \pm 17$  Hz is one of the highest for known atoll sources and is same within errors in both the observations. Also the XTE J1701-407 is one of the least luminous LMXB observed ( $L_x \sim 0.01 L_{\text{EDD}}$ ) in which kHz QPOs have been detected. The  $\sim 30$  Hz QPO detected in this source is not accompanied by broad components usually detected in other atoll as well as Z sources.

## Light Curve

Figure 1: Upper panel : Long term light curve of XTE J1701-407 obtained from the PCA galactic bulge scan monitoring observations. The 39 pointed observations of year 2008 were obtained in the time between the dashed vertical lines. 15 more observations in were obtained till 2011 in a number of campaigns. The arrows mark the approximate time and intensity of the observations in which kHz QPOs are detected.

## Color-Color Diagram

Figure 3: Colour-colour diagram of XTE J1701-401 using the 41 pointed observations. Arrows point to the observations in which kHz QPOs are detected. The soft state observations are the blue triangles. The hard state observations are shown in green circles.

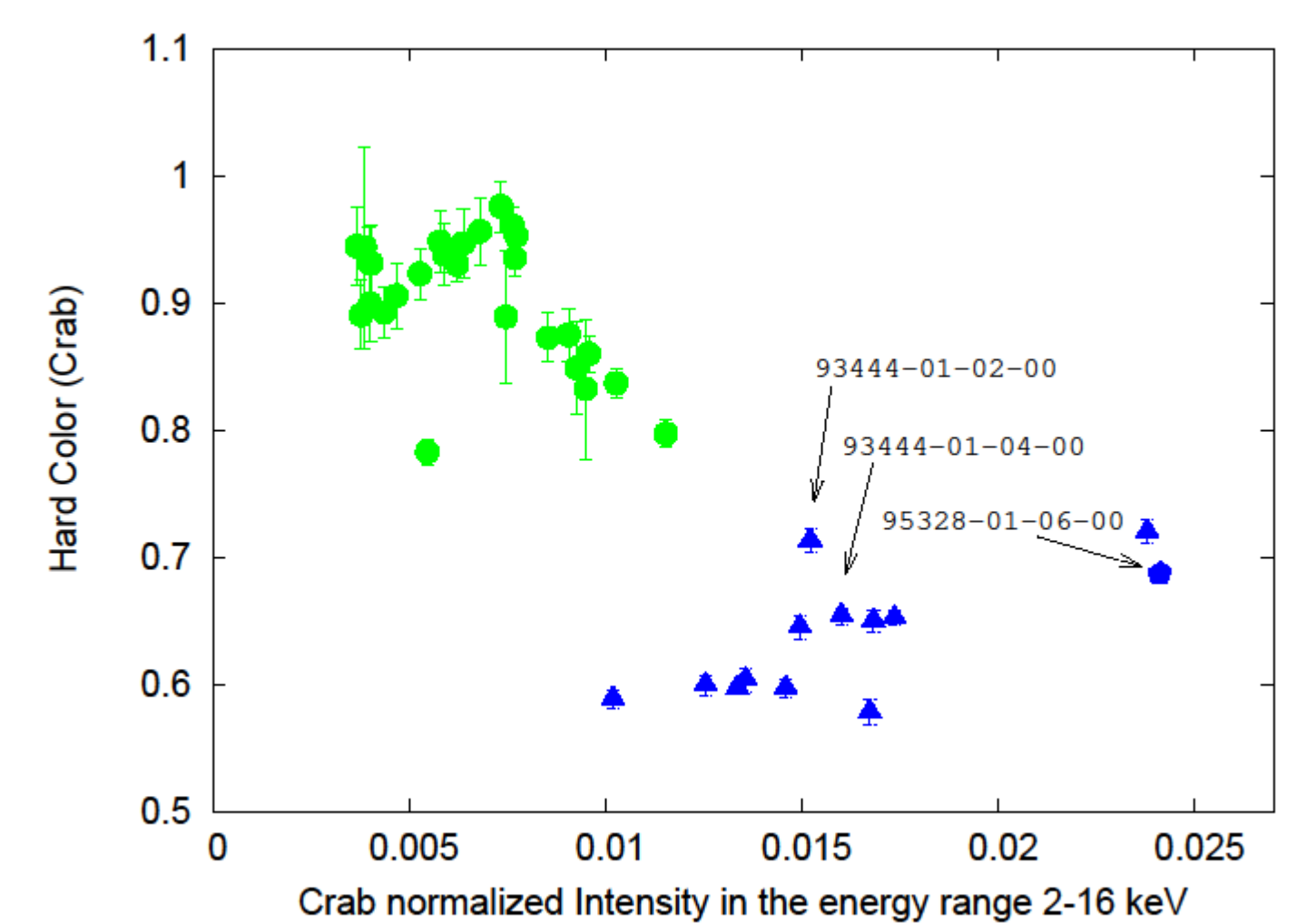


## 3 Year Outburst, and probably a new begins!!!

After a outburst of  $\sim 3$  years the source went into quiescence (below PCA detection level, see Atel #3604 of 2011/08/29) and within few days it was detected at  $\sim 142$  cts/s/5PCU on 2011/09/16. This may be the beginning of a new outburst.

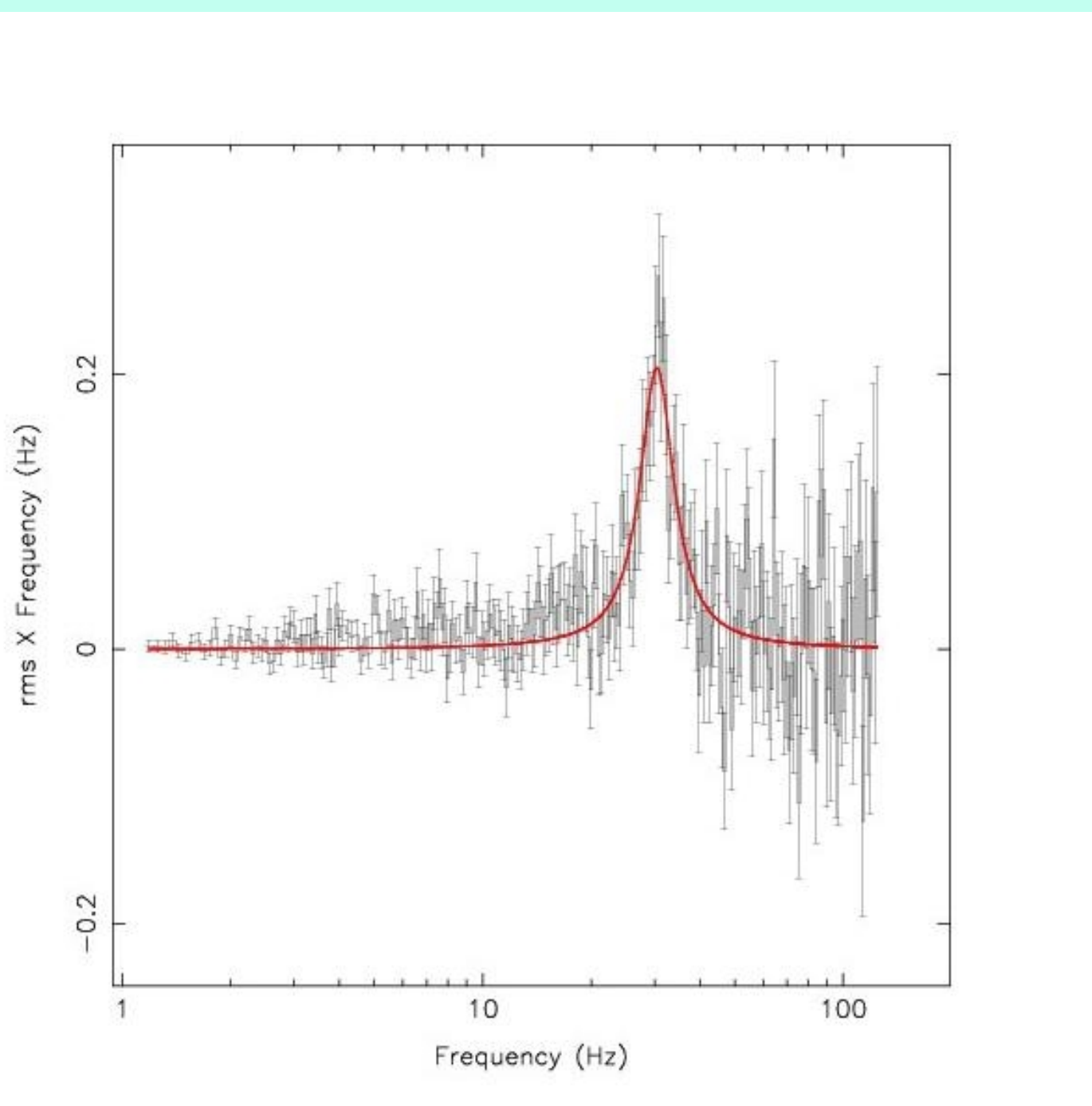
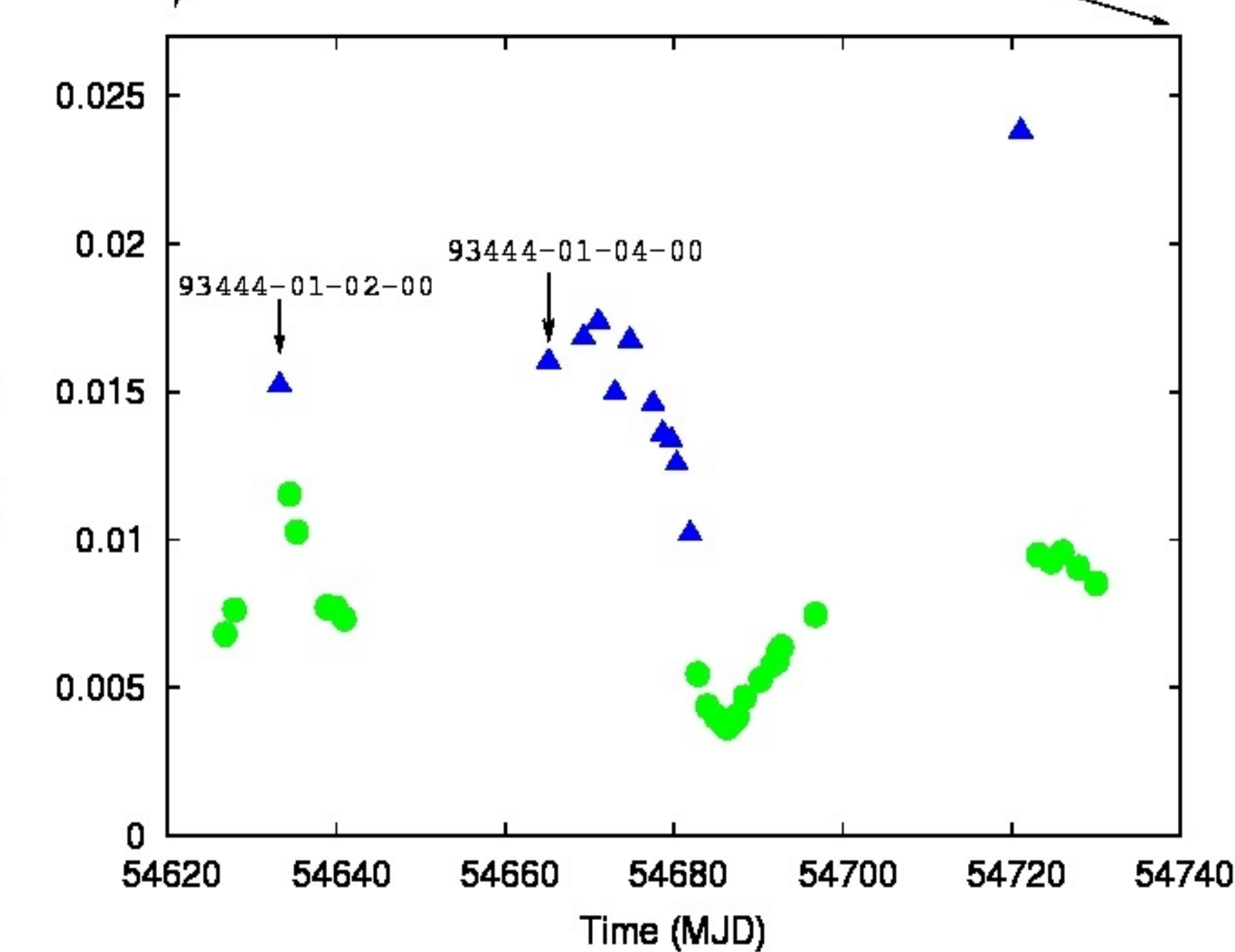
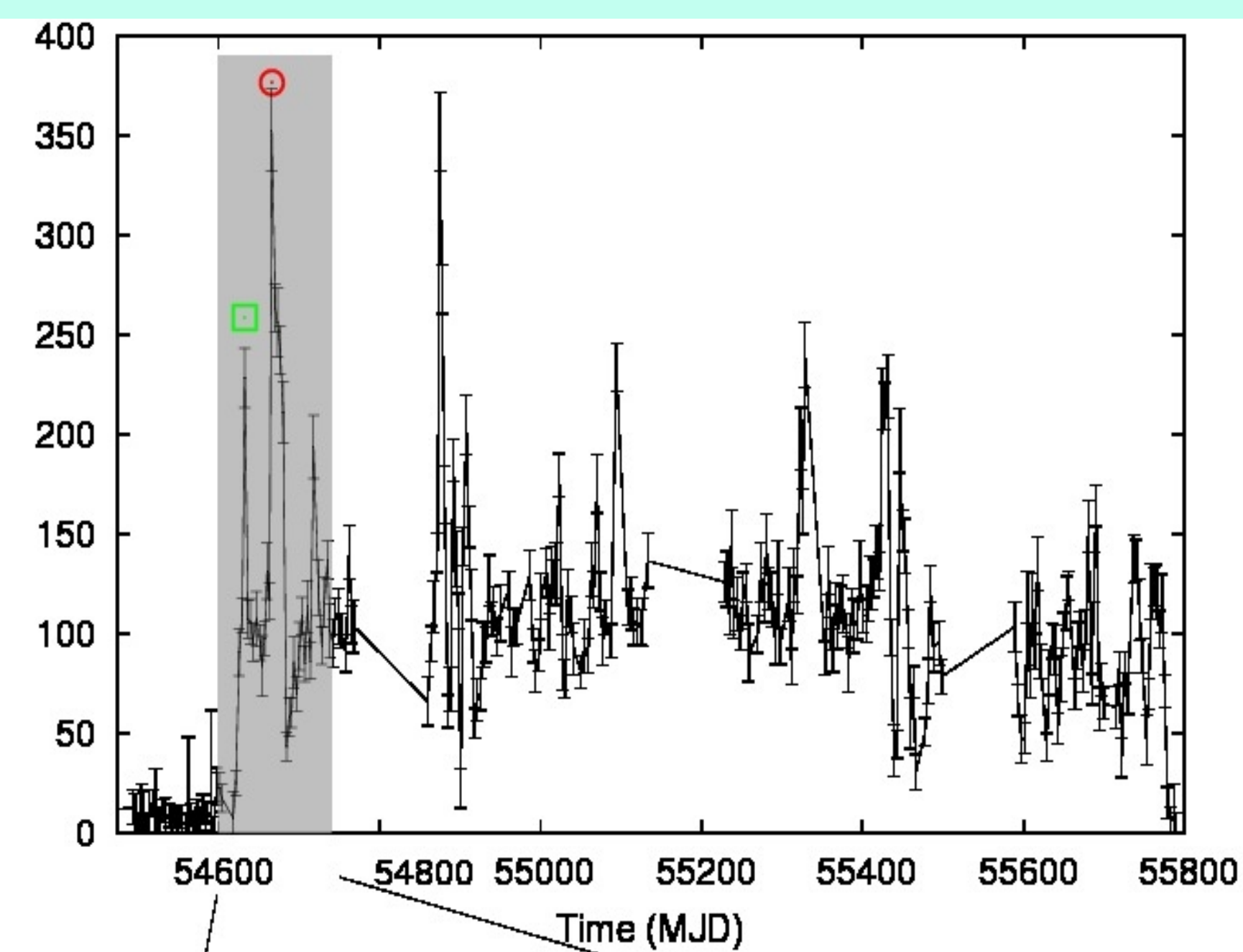
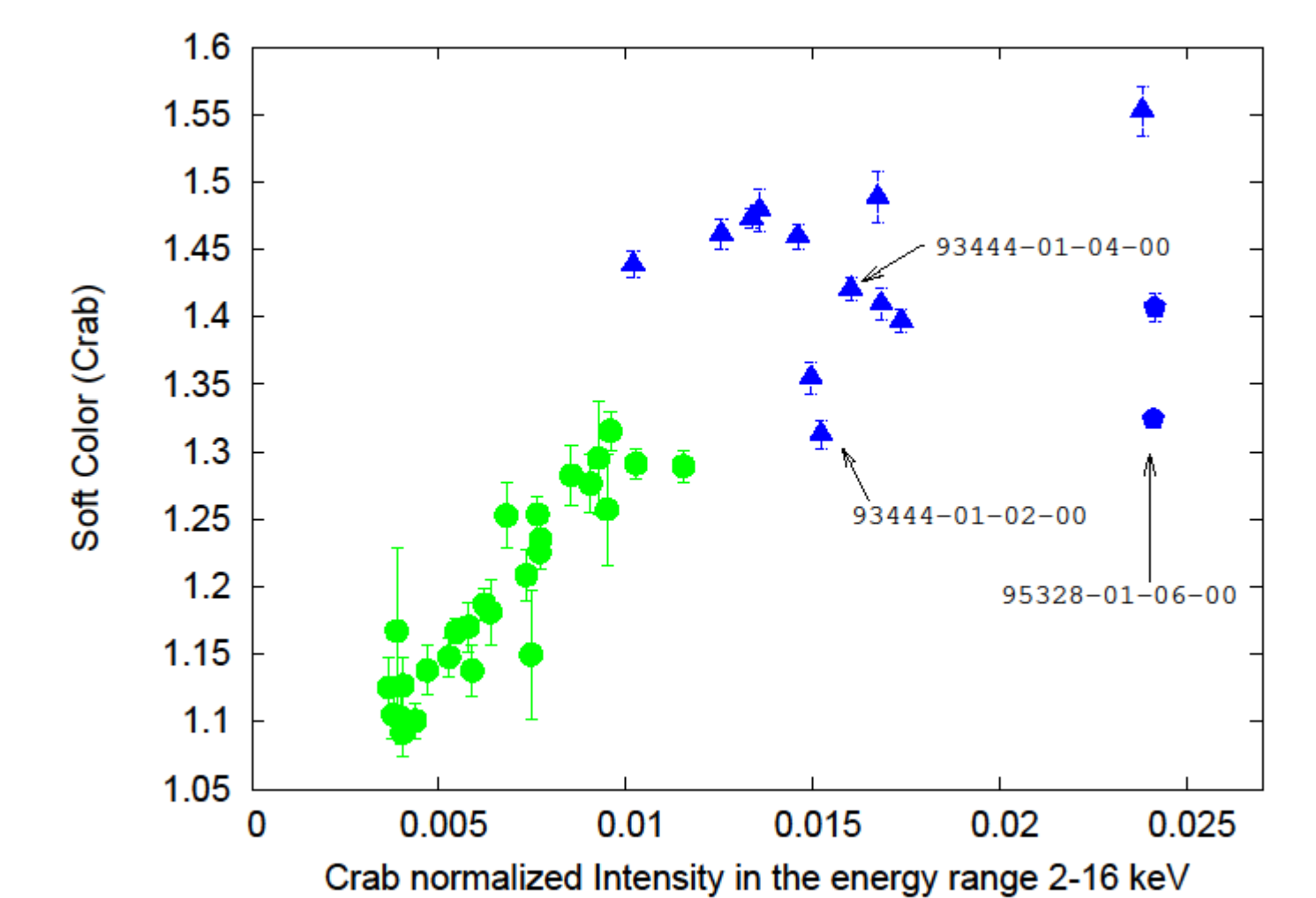
## Crab Normalized Light Curve

Figure 1: Lower panel : Crab normalized light curve of the 39 pointed observations of June to September 2008. The hard state observations are marked with green circles and soft state observations with blue triangles. The arrows mark the observations in which QPOs are observed.



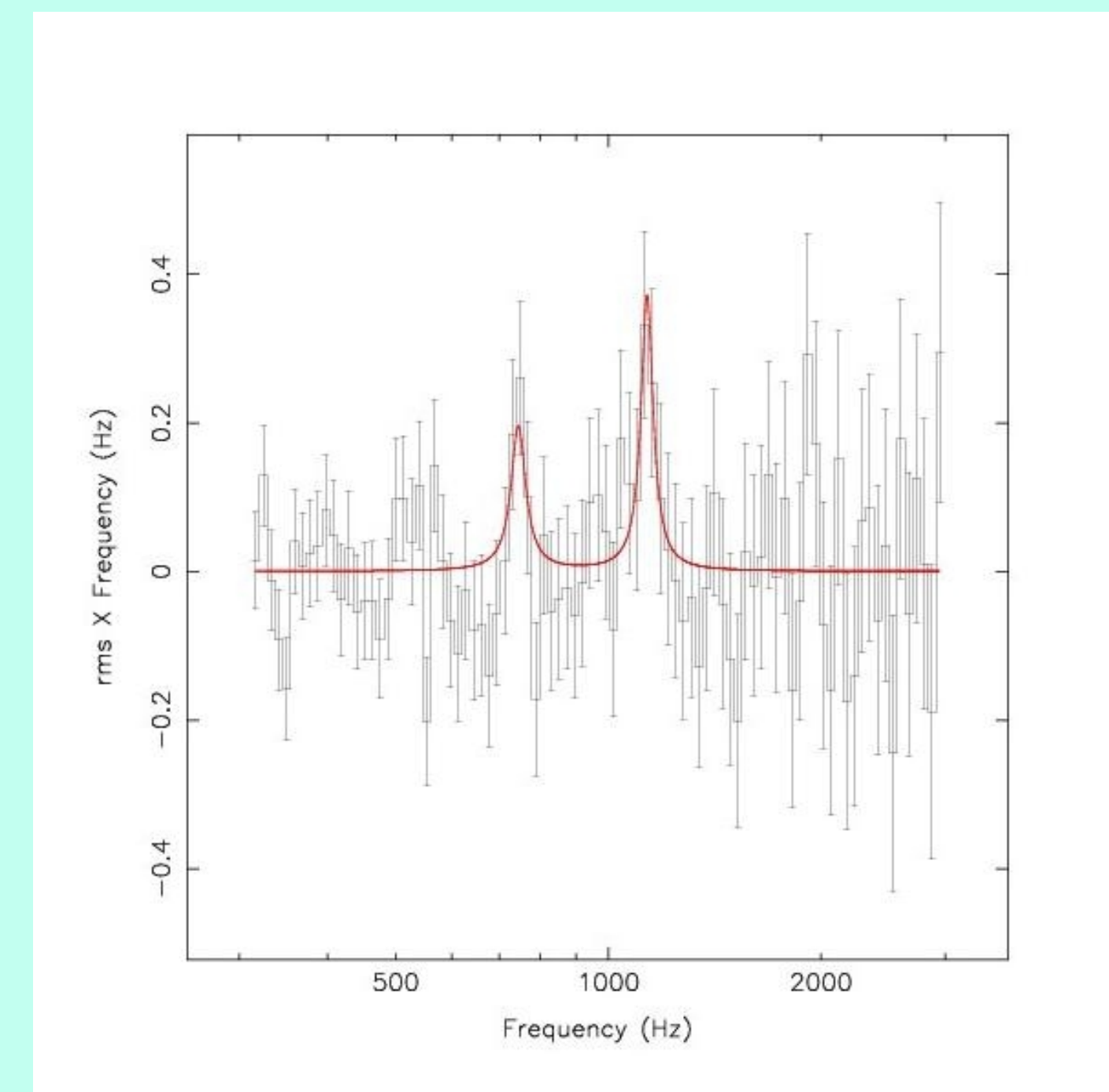
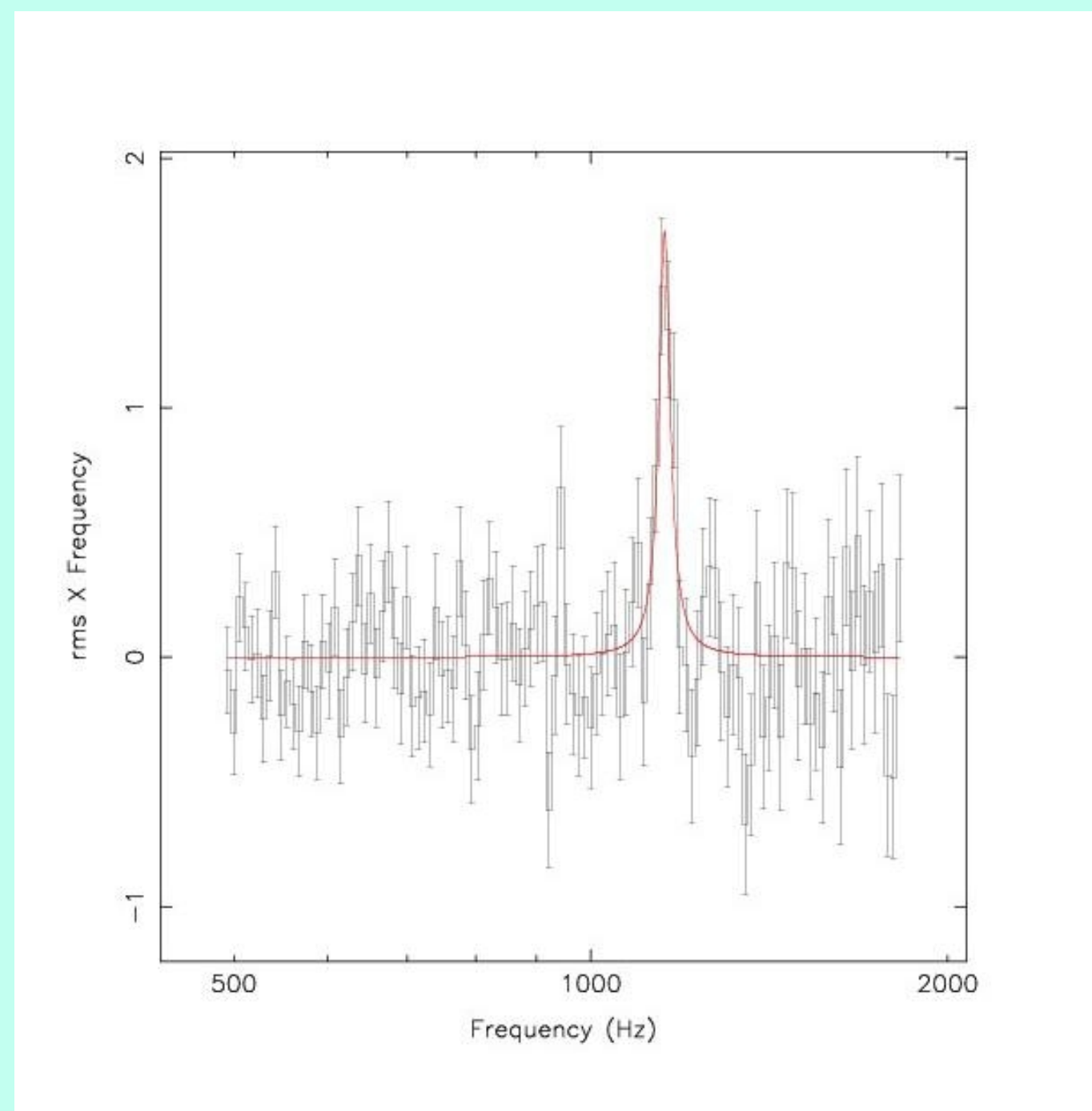
## Color-Intensity Diagram

Figure 4: Right panel is the plot of the soft colour with Crab normalized intensity in the 2-16 keV energy range. Left panel is the plot of hard colour with Crab normalized intensity in the 2-16 keV energy range. In this plot the spectrum is seen to become softer as the Luminosity increases.



## Quasi Periodic Observations

Figure 5: A  $\sim 30$  Hz QPO is detected in the observation 93444-01-02-00 dated 16<sup>th</sup> June 2008. This QPO is accompanied by a 1156 Hz QPO (see first panel of Figure 6).

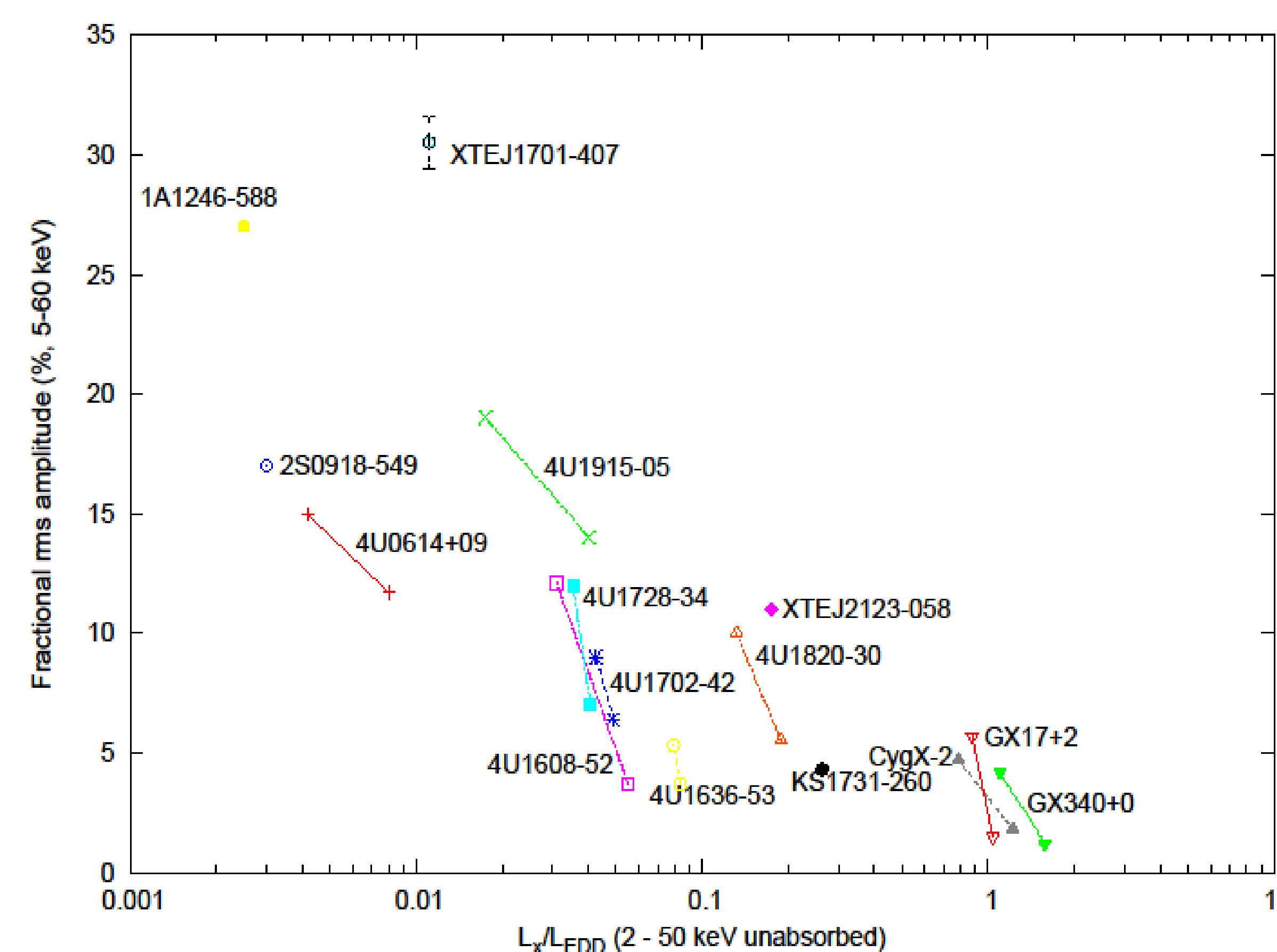


## kHz Quasi Periodic Observations

Figure 6: kHz QPOs have been detected in three observations. The first panel shows a 1156 Hz QPO detected in the observation 93444-01-02-00 dated 16<sup>th</sup> June 2008. In the observations 93444-01-04-00 dated 18<sup>th</sup> July 2008 and 95328-01-06-00 dated 17<sup>th</sup> August 2010 twin kHz QPOs were detected. The difference in the frequency of the twin kHz QPOs is  $\sim 370$  Hz. It is interesting to note that the frequency difference is same (within errors) for the two observations separated by  $\sim 24$  months. In case of the upper kHz QPO observed in 93444-01-04-00 (second panel), the root mean square (rms) amplitude is  $\sim 30\%$  in the 5-60 keV energy range. This is the highest rms observed in a kHz QPO in a low mass X-ray binary.

## Luminosity Vs fractional rms

Figure 7: Luminosity Vs fractional rms amplitude in the energy range 5 -60 keV of the upper kHz QPO in various LMXBs. There is a decrease in the fractional rms amplitude as the source luminosity increases, both within one source and between sources. In addition to the low luminosity atoll sources this plot also contains the following Z sources: Cygnus X-2, GX 17+2 and GX 340+0.



## Low Mass X-ray Binary XTE J1701-407

Discovery	8 <sup>th</sup> June 2008
Co-ordinates	17 <sup>h</sup> 01 <sup>m</sup> 53 <sup>s</sup> , -40 <sup>o</sup> 47'00".96
Distance	4 to 6 kpc

Some references for XTE J1701-407:

The Swift Capture of a long X-ray burst from XTE J1701-407, Linares M., Wijnands R., van der Klis M., A. W., P.S.P.D.N.C., R. S., 2009, MNRAS

The new intermediate long bursting source XTE J1701-407, Falanga M., Cumming A., Bozzo E., Chenevez J., Mar. 2009, A&A, 496, 333

RXTE Observations Of LMXB XTE J1701-407, D. Pawar, M. Kalamkar, D. Altamirano, K. Shanthi, D. Bhattacharya, (to be submitted in MNRAS)

ATel #3604; N. Degenaar, R. Wijnands, D. Altamirano (University of Amsterdam), et al.